Apparent thinning of human visual cortex during childhood is associated with myelination

Vaidehi S. Natu[a,b,1], Jesse Gomez[c], Michael Barnett[d], Brianna Jeska[a], Evgeniya Kirilina[e,f], Carsten Jaeger[e], Zonglei Zhen[a], Siobhan Cox[a], Kevin S. Weiner[g,h], Nikolaus Weiskopf[e], and Kalanit Grill-Spector[a,c,i]

[a]Department of Psychology, Stanford University, Stanford, CA 94305; [b]Department of Neurological Surgery, University of Texas Southwestern Medical Center, Dallas, TX 75390; [c]Neurosciences Program, Stanford University School of Medicine, Stanford, CA 94305; [d]Department of Psychology, University of Pennsylvania, Philadelphia, PA 19104; [e]Department of Neurophysics, Max Planck Institute for Human Cognitive and Brain Sciences, 04103 Leipzig, Germany; [f]Center for Cognitive Neuroscience Berlin, Free University Berlin, 14195 Berlin, Germany; [g]Department of Psychology, University of California, Berkeley, CA 94720; [h]Helen Wills Neuroscience Institute, University of California, Berkeley, CA 94720; and [i]Wu Tsai Neurosciences Institute, Stanford University, Stanford, CA 94305

Edited by David C. Van Essen, Washington University in St. Louis School of Medicine, St. Louis, MO, and approved August 27, 2019 (received for review March 30, 2019)

Human cortex appears to thin during childhood development. However, the underlying microstructural mechanisms are unknown. Using functional magnetic resonance imaging (fMRI), quantitative MRI (qMRI), and diffusion MRI (dMRI) in children and adults, we tested what quantitative changes occur to gray and white matter in ventral temporal cortex (VTC) from childhood to adulthood, and how these changes relate to cortical thinning. T_1 relaxation time from qMRI and mean diffusivity (MD) from dMRI provide independent and complementary measurements of microstructural properties of gray and white matter tissue. In face- and character-selective regions in lateral VTC, T_1 and MD decreased from age 5 to adulthood in mid and deep cortex, as well as in their adjacent white matter. T_1 reduction also occurred longitudinally in children's brain regions. T_1 and MD decreases 1) were consistent with tissue growth related to myelination, which we verified with adult histological myelin stains, and 2) were correlated with apparent cortical thinning. In contrast, in place-selective cortex in medial VTC, we found no development of T_1 or MD after age 5, and thickness was related to cortical morphology. These findings suggest that lateral VTC likely becomes more myelinated from childhood to adulthood, affecting the contrast of MR images and, in turn, the apparent gray–white boundary. These findings are important because they suggest that VTC does not thin during childhood but instead gets more myelinated. Our data have broad ramifications for understanding both typical and atypical brain development using advanced in vivo quantitative measurements and clinical conditions implicating myelin.

development | cortical thickness | quantitative MRI | diffusion MRI | longitudinal

As the brain develops from infancy to adulthood, magnetic resonance imaging (MRI) studies report that cortex appears to thin (1–6). Cortex in early sensory regions thins before higher-level frontal and temporal regions (1, 3). However, the mechanisms underlying cortical thinning during development are not well understood.

Three developmental theories have been proposed to explain apparent cortical thinning across development: Pruning, myelination, and cortical morphology. Pruning, evaluated using cross-sectional histological studies on postmortem brains, suggests that the removal of inefficient synapses, dendrites, and neurons leads to cortical tissue loss (7–9). Pruning is hypothesized to produce thinner cortex in adulthood and improve neural processing by optimizing brain circuits for particular operations. Myelination suggests that the myelin sheath wrapping axons grows during development (2, 10–13). This growth increases the efficiency of saltatory conduction and is thought to lead to faster and more reliable information transmission. Higher myelin content increases the intensity of voxels in T_1-weighted anatomical MR images. Thus, if voxels close to the gray–white matter boundary have less myelin in children, these voxels will appear darker than in adults, which may shift the apparent gray–white boundary deeper into the white matter in a child's brain (6, 14). A third possibility is that changes in cortical morphology (cortical folding and surface area [SA]) during childhood development may result in thinning. In particular, mechanical forces during development (15–17) may increase cortical sulcification and SA, which may result in a thinner cortex in adulthood (18). These mechanisms are not mutually exclusive as a combination of pruning, increased myelination, and morphological alterations may result in thinner cortex in adulthood.

Advances in quantitative MRI (qMRI) (19–21) and diffusion MRI (dMRI) (22) provide an exciting opportunity to measure noninvasively independent and complementary properties of gray and white matter tissue, thus allowing us to disambiguate developmental hypotheses in the living human brain. qMRI enables the measurement and comparison across individuals of the amount of nonwater tissue within a voxel (macromolecular tissue volume [MTV]) and the relaxation time (T_1), which depend on tissue composition (e.g., T_1 in myelinated tissue is lower than in unmyelinated tissue). Additionally, mean diffusivity (MD), obtained from dMRI, depends on the size, density, and structure of the space within tissue through which

Significance

MRI data suggest that the thickness of the human cortex appears to decrease during childhood development. However, the underlying microstructural mechanisms are unknown. Using multiple quantitative neuroimaging methods that are sensitive to microstructural tissue content, we found that gray matter tissue and its adjacent white matter in high-level visual cortex show tissue growth related to myelination. Increased myelin alters the contrast between gray and white matter in MRI images and, in turn, affects the apparent cortical boundary. These findings are important because they suggest that cortex does not thin during childhood but instead gets more myelinated. Our data impact understanding of typical and atypical brain development, and clinical conditions implicating myelin including dyslexia, autism, and multiple sclerosis.

Author contributions: V.S.N., J.G., and K.G.-S. designed research; V.S.N., J.G., M.B., B.J., E.K., and C.J. performed research; V.S.N., J.G., M.B., Z.Z., S.C., K.S.W., and K.G.-S. analyzed data; V.S.N. and K.G.-S. wrote the paper; E.K., C.J., and N.W. contributed to generation and analysis of histological data; and K.G.-S. contributed to all components of the study.

The authors declare no conflict of interest.

This article is a PNAS Direct Submission.

[1]To whom correspondence may be addressed. Email: vnatu@stanford.edu.

This article contains supporting information online at www.pnas.org/lookup/suppl/doi:10.1073/pnas.1904931116/-/DCSupplemental.

First Published September 23, 2019.

water diffuses, providing additional insight into microstructural changes during development (21, 23).

How can these MRI measurements differentiate the 3 developmental hypotheses? Although we cannot measure microstructure directly using in vivo MRI, we hypothesize that we can distinguish between developmental theories because their predicted effects on microstructure within a voxel differ. Pruning is associated with developmental reductions in synaptic spines, dendrites, and neurons (7). Although the effect of pruning on T_1 or MD are not fully understood, we hypothesize that pruning may lead to a reduction of macromolecular tissue volume fraction resulting in higher T_1 and MD in cortices of adults compared to those of children. In contrast, myelination predicts developmental changes to both white and gray matter. In the white matter, increased myelination predicts lower T_1 (19, 24) and reduced MD (21, 23). In the gray matter, myelination is pronounced in deep cortical layers closer to the gray–white boundary, as they contain more afferent and efferent projections than layers close to the pial surface (25, 26). Thus, in gray matter, development of myelin predicts lower T_1 (27, 28) and lower MD in cortices of adults compared to those of children, especially in deep layers. Finally, developmental changes in cortical morphology predict no developmental changes to either T_1 or MD of gray or white matter. Instead, this hypothesis predicts morphological changes in the local cortical curvature and SA.

To address developmental theories of cortical thinning, we obtained multiple independent measures of fMRI, qMRI, and dMRI in 27 children (ages 5 to 9, $n = 12$, 9 females; ages 10 to 12, $n = 15$, 5 females) and 30 adults (ages 22 to 28, $n = 30$, 11 females). We tested whether there are between-age group differences in T_1 and MD in ventral temporal cortex (VTC) and whether these developments are related to cortical thickness (CT) measurements in the same individuals.

We focused on VTC as a model system for studying the mechanisms of CT development for 3 reasons. First, accumulating evidence reveals differential functional and anatomical development across VTC, whereby face- and character-selective regions show prolonged development compared to place-selective regions (24, 27, 29–35). Thus, examination of the development of CT within VTC allows testing if apparent cortical thinning is guided by uniform or heterogeneous mechanisms across a cortical expanse. Second, functional regions within VTC can be identified without spatial smoothing in each participant's brain including children (27, 34, 35). This approach enables the examination of both the gray matter and its adjacent white matter in each individual, and increases the spatial precision of measurements compared to prior studies of cortical thinning, which examined large anatomical expanses spanning several centimeters (1–3). Third, cortical folding reliably predicts the location of functional regions in VTC with millimeter precision (36–39) in both children and adults. This structural–functional coupling in the VTC allows us to examine the relationship between CT and cortical morphology.

Results

We used fMRI to define functional regions of interest (fROIs) selective to faces, characters, and places in each participant's brain using a functional localizer experiment (*SI Appendix*, Fig. S1*A*). After localizing fROIs, we measured 1) CT of each fROI; 2) T_1 and MD in white matter adjacent to each fROI using qMRI and dMRI, respectively; 3) T_1 and MD in gray matter of each fROI across intracortical depths; and 4) cortical curvature of each fROI. We compared these measures across age groups to determine which factors develop and, if so, whether these developments are region-specific or region-general. Finally, we tested whether apparent cortical thinning is linked to development of T_1, MD, or curvature.

We first verified that data quality was not lower in children than adults. Due to excessive motion (>2 voxels) during fMRI, data from 3 out of 30 adults and 1 out of 27 children were removed from further analyses. In the remaining 11 children (ages 5 to 9), 15 preteens (ages 10 to 12), and 27 adults (ages 22 to 28), we found no between-group differences in motion and no correlation between motion and age ($R_{within} = -0.12$, P = ns; $R_{between} = -0.23$, P = ns; *SI Appendix*, Fig. S1*B*). Time series signal-to-noise ratio (tSNR) of fMRI data across VTC was higher in children than adults (tSNR correlation with age: $R_{LH} = -0.65$, $P < 0.01$; $R_{RH} = -0.70$, $P < 0.01$; *SI Appendix*, Fig. S1*C*). For dMRI, data from 2 children, 4 preteens, and 3 adults were excluded because of excessive motion above 2 voxels (1 voxel = $2 \times 2 \times 2$ mm^3), leaving 9 children (ages 5 to 9), 11 preteens (ages 10 to 12), and 24 adults (ages 22 to 28) for dMRI analyses. After these exclusions, there was no difference across age groups. These quality control analyses show that we can obtain high-quality measurements in children and that any developmental effects that we find are likely not due to nonspecific differences between age groups such as larger head motion or higher measurement noise in children than adults.

Using the localizer experiment, we defined fROIs in each participant that were selective for faces (pFus-faces and mFus-faces; also referred to as fusiform face area [FFA] 1 and 2, respectively) (40, 41), characters (pOTS-chars and mOTS-chars located in the occipital temporal sulcus [OTS]; also referred to as visual word form area [VWFA] 1 and 2, respectively) (42, 43), and places (CoS-places in the collateral sulcus [CoS]; also referred to as parahippocampal place area [PPA]) (44). We localized fROIs even in our youngest participants (Fig. 1*A* and *SI Appendix*, Table S1).

VTC Undergoes Apparent Thinning from Childhood to Adulthood. Maps of CT projected to each subject's cortical surface were generated using FreeSurfer (45) from T_1-weighted images. Our CT maps were consistent with prior ex vivo (46) and in vivo studies (2) (*SI Appendix*, Fig. S2). In general, CT decreased with age across VTC, except for a region near the temporal pole in which CT increased with age [interaction between age of subject and anatomical parcel, $F_{(16,900)} = 19.48$, $P < 0.05$; *SI Appendix*, *Methods* and Fig. S3 *A* and *B*].

Measurements of CT in fROIs of VTC showed that cortex appeared to thin from age 5 to adulthood in face-, character-, and place-selective regions [main effect of age, 3-way repeated-measures ANOVA with factors: Age of subject (5 to 9/10 to 12/22 to 28 y),

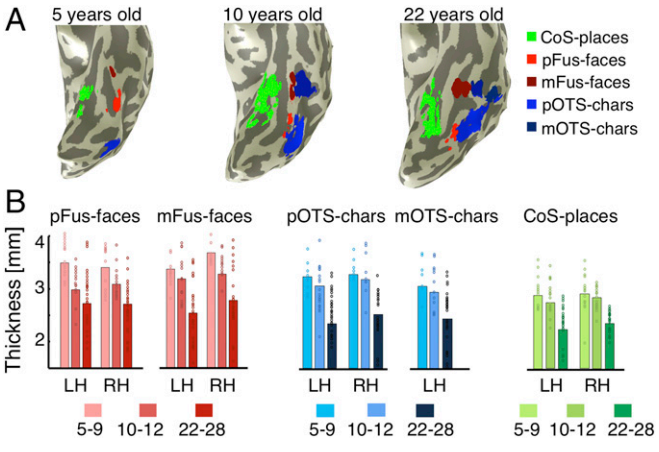

Fig. 1. Cortical thickness (CT) decreases from age 5 to adulthood in category-selective regions of ventral temporal cortex (VTC). (*A*) Functional regions in the left inflated VTC of 3 sample subjects, ages 5, 10, and 22 y. (*B*) Mean CT in face-selective regions in the lateral fusiform gyrus (pFus- and mFus-faces), character-selective regions in the occipito-temporal sulcus (pOTS- and mOTS-characters), and a place-selective region in the collateral sulcus (CoS-places) across children (ages 5 to 9, $n = 11$; 10 to 12, $n = 15$) and adults (ages 22 to 28 y, $n = 27$). CT is higher in children than adults in all fROIs. Bar height, mean CT; dots, individual subject's CT. LH/RH, left/right hemisphere.

fROI (face/place/character-selective), and hemisphere (left/right), $F_{(2,384)} = 78.74$, $P < 0.05$; Fig. 1*B*]. Children's cortex (ages 5 to 9) was on average 0.73 ± 0.11 mm thicker than adults'. The smallest difference was observed in right CoS-places (0.46 mm) and the largest difference in right mFus-faces (0.97 mm). Additionally, CT varied across fROIs [main effect of fROI, $F_{(2,384)} = 21.00$, $P < 0.05$], whereby cortex was thinnest in CoS-places (2.56 ± 0.45 mm), which lies close to the fundus of the CoS, and thickest in mFus-faces (2.97 ± 0.65 mm), which lies on the lateral fusiform gyrus (FG). There was also a small but significant hemispheric difference, as fROIs were thinner in the left than right hemisphere [$F_{(1,384)} = 4.99$, $P < 0.05$]. While cortex generally thins, not all fROIs showed volume decreases. We found developmental increases in the volume of face-selective regions [$F_{(2,206)} = 5.2$, $P < 0.05$] but not of character- or place-selective regions.

T_1 and MD Decrease from Childhood to Adulthood in Functionally Defined White Matter. As we found developmental changes in apparent CT, we first examined whether these developments were related to changes in white matter properties adjacent to each fROI. Thus, for each participant, we 1) generated whole-brain maps of T_1 and MD, and 2) measured mean T_1 and MD values in each participant's fROIs and the adjacent white matter. For the latter measurement, we extended gray matter fROIs into the adjacent white matter (Fig. 2*A* and *Materials and Methods*), which we refer to as functionally defined white matter (FDWM) (47). Then we evaluated mean T_1 (Fig. 2*B*) and MD (Fig. 2*C*) in FDWM of face-, character-, and place-selective fROIs in each participant. Results were similar for fROIs from the same domain and for different extensions of 2, 3, 4, and 5 mm into white matter. Thus, in subsequent main figures, we show a single fROI from each domain (face, mFus-faces; character, mOTS-chars; and place, CoS-places) that has been extended 5 mm into the white matter. Data from pFus-faces and pOTS-chars are in *SI Appendix*, Fig. S4.

Results show differential development of T_1 in FDWM [interaction between age of subject and fROI, $F_{(4,384)} = 2.54$, $P < 0.05$; Fig. 2*D* and *SI Appendix*, Fig. S4*A*]. T_1 progressively decreased from age 5–9 to 10–12 to adulthood in the FDWM near face- and character-selective regions (values of $F > 18.12$; values of $P < 0.05$). However, there was no change in T_1 in FDWM of place-selective cortex after age 5 [$F_{(2,98)} = 2.3$, P = ns]. In FDWM, where T_1 decreased with age, MTV concomitantly significantly increased with age (*SI Appendix*, Fig. S5).

There was also differential development of MD in FDWM [interaction between age of subject and fROI, $F_{(4,320)} = 4.64$, $P < 0.05$]. MD monotonically decreased in FDWM near face- and character-selective fROIs from age 5 to adulthood (values of $F > 8.77$, values of $P < 0.05$; Fig. 2*E* and *SI Appendix*, Fig. S4*B*). However, there was no development in MD of FDWM near CoS-places [$F_{(2,80)} = 2.57$, $P > 0.05$]. Decreases in both T_1 and MD in FDWM near face- and character-selective fROIs are consistent with the hypothesis that development of white matter near these fROIs is associated with increased myelination.

In Mid and Deep Cortical Depths, T_1 and MD Decrease from Childhood to Adulthood. Next, we tested whether cortical tissue properties develop from childhood to adulthood. We applied a data-driven approach, evaluating T_1 and MD in each fROI across cortical depths in equidistant steps extending from the pial surface into the white matter (10 steps for T_1 and 8 steps for MD; *SI Appendix*, Fig. S6). We used this approach for 2 reasons: 1) it enabled examining T_1 and MD values along the entire trajectory from the pial surface of the gray matter into the white matter, and 2) it allowed obtaining unbiased measurements that are independent of the classification of the tissue into gray or white matter by the segmentation algorithm.

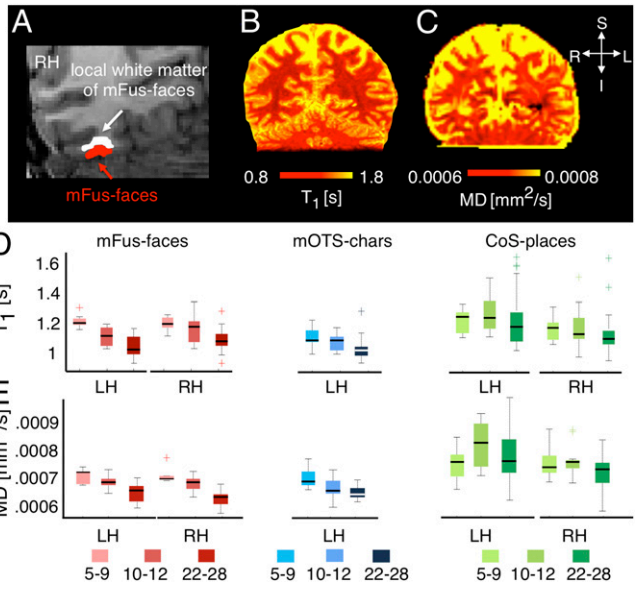

Fig. 2. Development of T_1 relaxation time and mean diffusivity (MD) in functionally defined white matter (FDWM) of VTC. (*A*) Section of a coronal slice showing face-selective mFus-faces (red) in the right hemisphere of a sample adult brain and its associated FDWM (white), which was generated by dilating the fROI 5 mm into the adjacent white matter. (*B* and *C*) Coronal slice in an example adult brain showing T_1 and MD maps, respectively. (*D*) Box plots showing median (thick line), 25th and 75th percentile (box), and range (whiskers) of T_1 across participants of each age group in bilateral mFus-faces (red), left mOTS-characters (blue), and bilateral CoS-places (green). Cross-hairs indicate outliers. T_1 progressively decreased from ages 5 to 9 ($n = 11$) to 10 to 12 ($n = 15$) to adulthood ($n = 27$) in face- and character-selective ROIs, but not in CoS-places. (*E*) Box plots showing MD in the same fROIs. MD also decreased from ages 5 to 9 ($n = 9$) to 10 to 12 ($n = 11$) to adulthood ($n = 24$) in face- and character-selective ROIs, but not in CoS-places. Light colors, 5- to 9-y-olds (yo); medium colors, 10- to 12-yo, and dark colors, 22- to 28-yo. LH/RH, left/right hemisphere.

Results revealed 2 main findings. First, examination of T_1 curves across cortical depth showed that T_1 near the gray–white matter boundary was lower than T_1 in superficial layers of gray matter (Fig. 3*A*). Second, across cortical depths, in face- and character-selective fROIs, the largest development in T_1 occurred away from the superficial pial surface and was prominent in mid cortical depths (Fig. 3*A*, mFus-faces and mOTS-chars; *SI Appendix*, Fig. S7*A*, pFus-faces and pOTS-chars). In contrast, in CoS-places, T_1 curves largely overlapped across age.

Notably, in face- and character-selective regions, T_1 curves were shifted leftward in adults compared to children. In other words, comparable T_1 values were deeper (closer to the white matter) in children than adults (Fig. 3*A*). For example, T_1 at the gray–white boundary in 5- to 9-y-olds was equivalent to T_1 at ~80% depth in adults. To quantify this shift, we fitted a local logistic function to each subject's T_1 curve, and estimated the slope and inflection point (which reflects the depth at which the slope is maximal). Results revealed that the depth of this inflection point was closer to the white matter in children than adults (Fig. 3*B*). There was larger development in face- and character-selective fROIs than in place-selective fROIs [interaction between age of subject and fROI, $F_{(4,384)} = 3.89$, $P < 0.05$]. There was also a development in the slopes [main effect of the age, $F_{(2,384)} = 49.65$, $P < 0.05$] as the slopes were steeper in children than adults. Development of slopes trended to be larger in face- and character-selective fROIs than in place-selective fROIs [interaction between age of subject and fROI, $F_{(4,384)} = 2.05$, $P = 0.08$].

To test whether differences in T_1 could be due to between-group differences in fROI size, we repeated the analyses using

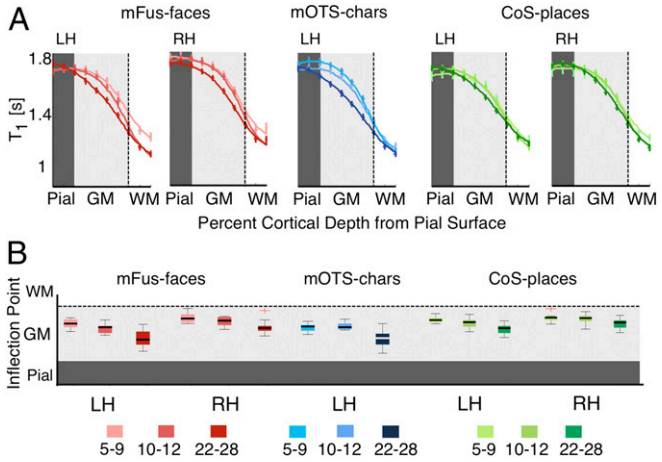

Fig. 3. Development of T_1 in gray matter as a function of cortical depth. (*A*) T_1 curves across equidistant intracortical depths from the pial surface (pial), to gray matter (GM) and into adjacent white matter (WM) in bilateral mFus-faces (red), left mOTS-characters (blue), and bilateral CoS-places (green) across age groups. Error bars indicate SEM. Dark- to light-gray transition line indicates pial–gray boundary estimates from FreeSurfer. Apparent gray–white matter boundary is indicated by the dotted line on the right edge of the gray zone. Two ticks to the right of this boundary indicate 2 steps into local WM. (*B*) Box plots of the inflection point of T_1 curves across age groups. The inflection point reflects the cortical depth at which slope of the T_1 curve is maximal. LH/RH, left/right hemisphere.

constant size ROIs of 5-mm radius centered on the centroid of each fROI. Results remained unchanged. There was differential development in the inflection point of T_1 data across depth, with larger development in face- and character-selective fROIs than in place-selective fROIs [interaction between age of subject and fROI, $F_{(4,384)} = 4.04$, $P < 0.05$] and a trend for steeper slopes in children's T_1 data in face- and character-selective fROIs than place-selective fROIs [interaction between age of subject and fROI, $F_{(4,384)} = 1.98$, $P = 0.09$].

The development of MD across cortical depths is more complex than the development of T_1 (*SI Appendix*, Figs. S7*B* and S8*A*). Across age groups, MD decreased from the pial surface to the white matter. To quantify development in MD curves, we fitted a linear function to each subject's MD curve and estimated slopes. Slopes were steeper in adults' fROIs compared to children's [main effect of the age, slope: $F_{(2,320)} = 17.41$, $P < 0.05$]. Within face-selective fROIs, MD development was observed in deeper cortical layers and the adjacent white matter rather than superficial layers (*SI Appendix*, Figs. S7*B* and S8*A*), but in the place-selective fROI, development was mainly driven by differences in MD at the pial surface. Indeed, there was a development of the intercept of the MD line fit of place-selective fROI [$F_{(2,80)} = 8.72$, $P < 0.05$], but not of face- or character-selective fROIs (values of $F < 2.2$, values of P = ns). Together, results show that T_1 and MD in lateral VTC decrease with age, suggesting microstructural tissue growth and not tissue loss in gray matter.

Does Tissue Growth in Face- and Character-Selective Regions Correlate with Apparent Cortical Thinning? We reasoned that if apparent cortical thinning relates to development in tissue properties, then there would be a positive correlation between CT and T_1 (or MD). We quantified the relationship between CT and T_1 (or MD) across each cortical depth per fROI. In face- (bilateral pFus-faces and mFus-faces) and character-selective fROIs (bilateral pOTS-chars and left mOTS-chars), CT and T_1 were positively correlated (values of $R > 0.48$, values of $P < 0.05$), as were CT and MD (values of $R > 0.36$, values of $P < 0.05$). The highest correlation was between CT and T_1 at ∼50% cortical depth from the pial surface (Fig. 4) and between CT and MD at ∼80% cortical depth (*SI Appendix*, Fig. S8*B*). The correlation between CT with T_1 remained significant after partialing out age (Fig. 4; same for MD, *SI Appendix*, Fig. S8*B*). In CoS-places, where we did not find development of tissue properties, we also did not find a correlation between CT and T_1 (right CoS-places, $R = 0.3$, P = ns) or CT and MD except for a correlation between CT and T_1 at ∼50% depth in left CoS-places ($R = 0.47$, $P < 0.05$; significant after age partialed out). Together, these analyses suggest that, in mid and deep cortical depths of face- and character-selective fROIs, participants with more tissue (lower T_1 and MD) have an apparent thinner cortex.

Do Developments in CT and Tissue Growth Occur Longitudinally in Children? We reasoned that if cross-sectional data reveals cortical thinning and tissue growth cross-sectionally, then there may be longitudinal anatomical changes in CT and T_1 within functionally and anatomically defined cortical regions localized in an individual child. To test this possibility, we obtained a second set of qMRI data from ∼70% of our child participants (n = 18/26) after an average of 1.42 ± 0.15 y. We examined how CT and T_1 of anatomical regions and fROIs varied across time within the same individual.

Results revealed 2 main findings. First, we found apparent cortical thinning from the first to second time points in anatomical ROIs of VTC [main effect of time in a 3-way ANOVA using as factors: time (year1/year2), anatomical ROI (FG/CoS/OTS), and hemisphere (left/right), $F_{(1,204)} = 35.4$, $P < 0.0001$; *SI Appendix*, Fig. S9]. Anatomically, we observed larger cortical thinning in children's FG ($Mean_{CTchange}$: 0.23 ± 0.05 mm) and CoS ($Mean_{CTchange}$: 0.22 ± 0.05 mm) than in the OTS ($Mean_{CTchange}$: 0.06 ± 0.06 mm) across these 2 time points [interaction between fROI and year, $F_{(2,204)} = 4.64$, $P < 0.05$]. This longitudinal thinning is consistent with prior studies (2). Second, we observed a longitudinal decrease in T_1 in fROIs of the VTC [main effect of time in a 3-way ANOVA with factors time (year1/y2), fROI (face-, place, and character-selective fROIs), and hemisphere (left/right): $F_{(1,252)} = 6.37$, $P < 0.01$; Fig. 5]. This suggests longitudinal tissue growth within children's VTC. Importantly, significant (values of $F > 3.17$, values of $P < 0.05$) growth occurs in face- ($Mean_{T1change}$ = 0.034 s ± 0.01 s) and character-selective fROIs ($Mean_{T1change}$ = 0.045 ± 0.006 s), where we observed cross-sectional reduction of T_1 from childhood to adulthood. However, there were no longitudinal changes in T_1 in the place-selective fROI [$F_{(1,64)} = 0.4$, P = ns].

What Cellular Mechanisms Underlie Tissue Growth in Face- and Character-Selective fROIs? We hypothesized that one tissue compartment that could affect cortical development of T_1 and MD might be myelin. However, there is lack of knowledge regarding myelination in VTC and its functional subdivisions. Addressing this gap in knowledge requires measurements of myelin in histological tissue slices of postmortem brains.

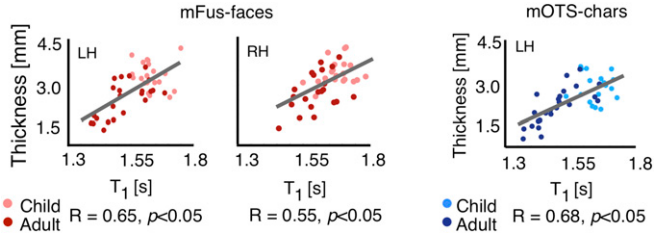

Fig. 4. T_1 in midcortical depths in face- and character-selective areas correlates with CT. Red, scatter plot showing a positive correlation between CT of mFus-faces and T_1 at midcortical depth (∼50% projection into gray matter). Blue, same for left mOTS-characters. Each point reflects data from one participant. Lighter colors represent children.

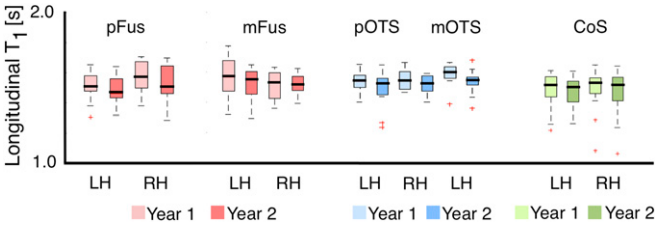

Fig. 5. Longitudinal development of T_1 in children's VTC. Box plots showing median (thick line) T_1 in year 1 (light colors) and year 2 (dark colors) in 18 children in face- (in red), character- (in blue), and place-selective cortex (in green). LH/RH, left/right hemisphere.

We examined the effect of myelin on in vivo measures of CT using postmortem analyses of human VTC. Due to its rarity, we were unable to obtain pediatric postmortem tissue to measure myelin development. Therefore, we leveraged tissue differences across fROIs in adults as a proxy. Specifically, our results also revealed that, in adults, relaxation rate ($R_1 = 1/T_1$) was significantly higher in face-selective fROIs (bilateral pFus-faces and left mFus-faces) than in CoS-places (values of $t > 2.39$, values of $P < 0.05$; Fig. 6*A*). However, in children, there was no difference in T_1 between face- and place-selective fROIs (values of $t < 0.57$, values of $P > 0.05$). In other words, tissue within face- and place-selective regions is undifferentiated in childhood, and development leads to differentiated R_1 in face- and place-selective fROIs in adulthood. We reasoned that if myelin contributes to R_1 development, then in adults, face-selective cortex should be more myelinated than place-selective cortex.

To identify these regions in postmortem histological slices, we need anatomical markers. Prior research from our laboratory identified reliable anatomical landmarks that predict face-selective and place-selective fROIs in VTC: The midfusiform sulcus (MFS) predicts face-selective regions (37) and the intersection of the anterior lingual sulcus and the CoS predicts CoS-places (38) (Fig. 6*B*). We did not include character-selective fROIs on the OTS, as their locus is less predictable from anatomical landmarks compared to face- and place-selective fROIs.

To maximize the correspondence between postmortem histology and fMRI data, we identified anatomical landmarks for face- and place-selective fROIs in 30-μm-thick coronal slices from 5 postmortem brains containing FG, MFS, CoS, and calcarine sulcus (Fig. 6*C*). Then, we stained histological coronal slices containing these landmarks for myelin using a modified Gallyas stain (48). Myelin content was estimated from optical density (OD), which indicates the index of light refracted through the tissue (more myelin produces a darker stain; Fig. 6*D*).

Myelin-stained coronal slices revealed striking laminar differences across cortex (example: Fig. 6*D*; all brains: *SI Appendix*, Fig. S10). Deeper cortical layers had more myelin than superficial layers. The differentiated pattern is also evident in the high-resolution (50-μm) T_2*-weighted MR image of the same brain (Fig. 6*E*). We note 2 interesting observations (1): Highly myelinated cortex in VTC extends from the white matter boundary to about ~54% of the cortical depth in the FG, but only ~36% into cortex in the CoS. This estimate is consistent with prior findings using an equivolume model of cortical folding (49, 50), which considers the different curvatures across the FG and CoS (2). The density of myelin is higher (darker stains) in the FG than in the CoS (Fig. 6*D*).

We quantified these observations by measuring normalized OD profiles along equidistance depths from the pial surface to white matter for FG/MFS and CoS in each postmortem brain. Myelin content increased from superficial layers to deep cortical layers (Fig. 6*F*). Importantly, in 4 out of 5 brains, myelin content in the FG/MFS was greater than in the CoS away from the pial surface (Fig. 6*F*). Results are largely consistent with in vivo R_1 data (Fig. 6*A*).

Thus, using histological analyses of myelin in FG/MFS and CoS, we show that myelination is a likely mechanism underlying differences in adult in vivo T_1 measurements across these regions. Although we did not examine pediatric postmortem data, results are consistent with the idea that higher myelination in adult face- than place-selective cortex is due to developmental increases in myelin.

Cortical Curvature and Surface Area Are Linked to Developmental Thinning in CoS Places. Our qMRI and dMRI measurements did not find developments in microstructural tissue properties of CoS-places, even as it appears to thin from age 5 to adulthood (Fig. 1*B*). Thus, we asked whether apparent cortical thinning in CoS-places is linked to morphological changes including changes in cortical curvature and surface area (SA). Analysis of cortical curvature revealed that adults' CoS-places was on a more concave surface compared to children's CoS-places [main effect of age with factors age of subject and hemisphere, $F_{(2,98)} = 3.47$, $P < 0.05$; Fig. 7*A*]. Notably, we found a significant negative correlation between CT and curvature in CoS-places (Fig. 7*B*, *Right*, $R = -0.43$, $P < 0.05$, which was also significant when age was partialed out; Fig. 7*B*, *Left*, $R = -0.34$, $P < 0.05$, ns when age partialed out). That is, more concave CoS-places was associated with thinner cortex. In contrast, there was no development in the curvature of face- or character-selective fROIs (values of $F < 1.45$, values of $P =$ ns), and no correlation between CT and curvature in bilateral pFus-faces, mFus-faces, and left pOTS-chars (values of $R > -0.3$, values of $P > 0.05$). However, there was a negative correlation between CT and curvature in left mOTS-chars and right pOTS-chars

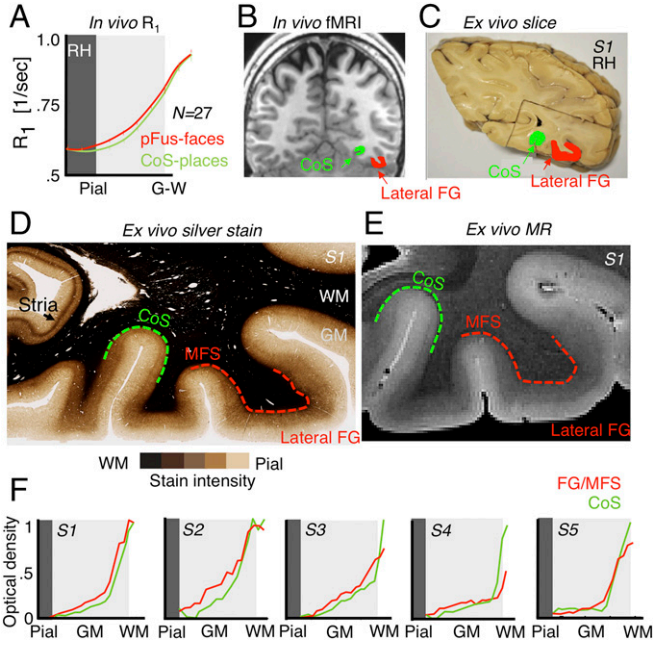

Fig. 6. Validation of adult in vivo data using adult postmortem myeloarchitecture. (*A*) In vivo measurement of relaxation rate ($R_1 = 1/T_1$[1/s]) shows greater R_1 in *Right* pFus-faces than CoS-places in *Middle* and deep cortical layers across 27 adults. Error bars indicate SEM. (*B*) In vivo example adult coronal slice showing the location of pFus-faces (red) and CoS-places (green) with respect to the midfusiform sulcus (MFS), fusiform gyrus (FG), and collateral sulcus (CoS). Right hemisphere is on the *Right* side. (*C*) Photograph of a postmortem section of subject (S1) showing tissue block used for histology. Green, CoS; red, lateral FG. (*D*) A sample (30-μm-thick) histological section (subject: S1) stained with modified Gallyas stain for myelin. Dashed red, FG/MFS; dashed green, CoS. (*E*) High-resolution (50 μm) T_2*-weighted image of section in *D* showing differentiation of MR contrast measures across cortex consistent with myelin stain in *D*. (*F*) Measurements of optical density across cortical depths in 5 postmortem brains along the CoS and FG/MFS.

(values of $R < -0.33$, values of $P < 0.05$; significant when age was partialed out). These results suggest that adults' thinner CoS-places might be located in a morphologically different location than children's thicker CoS-places.

To explore this prediction, we visualized the location of CoS-places on the cortical sheet by generating group maps of CoS-places in children ($n = 26$) and adults ($n = 27$) using cortex-based alignment to the FreeSurfer average brain. As shown in Fig. 7*C* for the right hemisphere, the location of CoS-places in children is more variable along the lateral–medial axis of the CoS compared to adults. We highlight that this developmental shift in the cortical location of place selectivity within the CoS is not due to statistical threshold as it is also observed in unthresholded group average maps (*SI Appendix*, Fig. S11). To explore whether additional metrics are morphologically different in CoS-places between children and adults, we examined the volume and SA of CoS-places in children and adults, with 2 main findings. First, we found no developmental changes in the volume of CoS-places [$F_{(2,98)} = 0.39$, P = n.s.]. Second, we examined 1) if the SA of the CoS increases during development (52), and 2) if larger SA is coupled with thinner cortex. We derived in each subject the CoS from FreeSurfer's anatomical parcellation, and evaluated whether its SA (in square millimeters) correlates with its CT. Area of the CoS expands with age [main effect of age, $F_{(2,100)} = 4.07$, $P < 0.05$; Fig. 7*D*] and was negatively correlated with CT in both hemispheres (values of $R < -0.41$, values of $P < 0.05$; significant when age partialed out). Thus, these results suggest that apparent thinning in CoS-places may be linked to morphological changes in curvature and SA of the CoS.

Apparent vs. Veridical Cortical Thickness: Is the Estimate of the Gray–White Matter Boundary from in Vivo Measurements Different from the Veridical Gray–White Boundary? A final question is how well does apparent CT obtained from MR measurements correspond to the actual thickness of human cortex in VTC? CT estimates from MRI are based on the definition of the gray–white boundary.

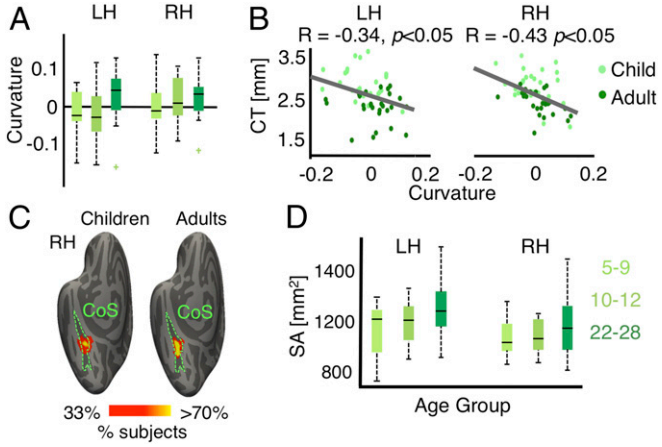

Fig. 7. CT of CoS-places is linked to development in cortical curvature. (*A*) Box plots showing median (think line) curvature across participants of each age group in bilateral CoS-places. Positive numbers indicate more concave surfaces (sulcal folds), and negative numbers indicate convex surfaces (gyral folds). (*B*) Scatterplot and correlation between CT and curvature of CoS-places. Each dot represents a participant. (*C*) Probabilistic group maps of the right CoS-places in children and adults. Color indicates percentage of participants in which each vertex is included in their CoS-places. Data are shown on the FreeSurfer average cortical surface (51). Location of CoS-places in adults is less variable than children, along the lateral-medial axis of CoS. (*D*) Box plots showing median (thick line) surface area (SA) across participants per group in bilateral CoS. SA increases from age 5 to adulthood. Lighter colors represent children. LH/RH, left/right hemisphere.

This boundary depends on the difference in T_1 of white and gray matter, which is coupled with myelin content. Any misestimates of this boundary will lead to inaccuracies in estimating CT from MRI measurements. The gray–white boundary in our MR images may deviate from the actual gray–white boundary for several reasons: 1) 1-mm voxels can contain multiple tissue types, which may lead to inaccuracies in labeling a voxel to white or gray matter (53); 2) voxel intensity based on R_1 ($R_1 = 1/T_1$) may not precisely follow the myelin transition from gray to white matter; and 3) the gray–white boundary determined from myelin may be less precise than one measured based on cell bodies.

To address these issues, we first benchmarked our measurements of CT in adult VTC relative to MRI data acquired at 0.7-mm resolution from the Human Connectome Project (HCP) (54) and Zaretskaya et al. (55). Differences in apparent CT across studies are in the range of 0.1 to 0.2 mm (*SI Appendix*, *Analysis of CT from MRI Data Obtained at 0.7 mm Resolution*). Second, we obtained veridical measurements of CT in histological slices of 4 adult postmortem brains (same as data as Fig. 6 and *SI Appendix*, Fig. S10; 4 out of 5 brains were used due to availability of all of the following datasets) using 1) a Nissl stain for cell bodies (30-μm resolution; Fig. 8*A*), 2) a silver stain for myelin (30-μm resolution; Fig. 8*B*), 3) R_1 imaging at 200 μm (Fig. 8*C*), and 4) resampled R_1 data to 1 mm (Fig. 8*D*). We measured CT (distance in millimeters between the pial surface and gray–white boundary) at multiple points along the cortical folds of the FG/MFS and CoS (see sample Nissl stain in *SI Appendix*, Fig. S12) and then averaged all measures within a region to obtain the average CT for that brain and region.

Results show that CT measured at 30-μm resolution based either on cell bodies or myelin yields similar values (Fig. 8*E*, no main effect of measurement in a 2-way ANOVA with factors measurement type [cell body/myelin] and fROI [FG/CoS]: $F = 0.01$, P = ns; see *SI Appendix*, Fig. S13 for boundary estimates on Nissl stains). Estimates of CT from R_1 at 200 μm are slightly lower (0.14 ± 0.10 mm) than from histology measures (Fig. 8*E*; trend for a main effect of data type in a 2-way ANOVA with factors data type [histology/MR] and fROI [FG/CoS]: $F = 3.25$, $P = 0.08$), but are not different from R_1 measurements resampled to 1 mm (Fig. 8*E*, no main effect of resolution [200 μm/1 mm]: $F = 0.02$, P = ns) even as the boundaries are not identical. Finally, we evaluated potential differences in measurements due to tissue shrinkage between histological sections and MRI images using corresponding vascular landmarks on myelin-stained histological slices and 50-μm MRI data of the same brains (*SI Appendix*, Fig. S14). Results revealed a 4.22% ± 2.2% (mean ± SD) difference, equivalent to a 0.10- to 0.13-mm measurement error in CT estimates. This measurement error is within our observed measurement error of CT across all data types.

Together, these data suggest that, in adults, estimates of CT from 1-mm T_1-weighted image closely match the actual CT. However, our data suggest that CT estimates from T_1-weighted imaging in children's brains may overestimate CT values because both our cross-sectional (Figs. 2 and 3) and longitudinal data (Fig. 5) show higher T_1 of the gray and adjacent white matter of face- and character-selective regions in younger participants.

Discussion

We combined fMRI, qMRI, and dMRI in children and adults, and histology in postmortem data, to understand the mechanisms underlying development of CT in VTC during childhood, with 3 main findings. First, in face- and character-selective regions, T_1 and MD decreased from childhood to adulthood. Both of these changes occurred in mid and deep gray matter depths and in the adjacent white matter. Complementary longitudinal measurements in the same children revealed a decrease in cortical T_1 in the same fROIs over a course of ∼1.5 y. These changes are consistent with increases in myelination of face- and character-selective VTC fROIs and their adjacent white matter after age 5.

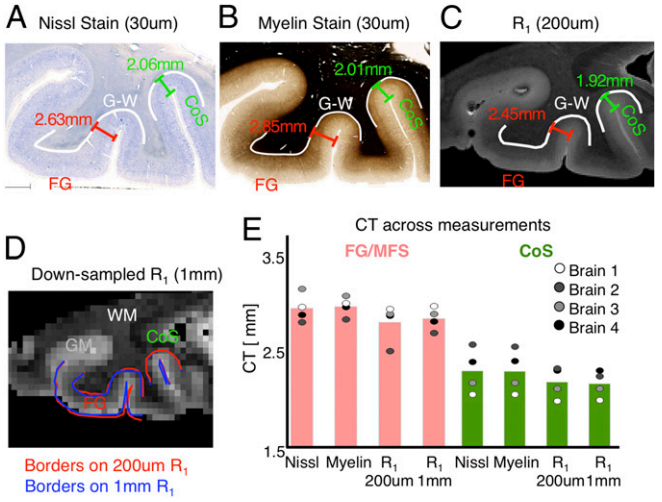

Fig. 8. Comparison of veridical and MR estimates of CT in postmortem samples. (*A*) Nissl stain of cell bodies, (*B*) silver stain for myelin, and (*C*) quantitative R_1 relaxation rate ($1/T_1$) of a sample coronal slice of a postmortem brain showing sample CT measures along points on the surfaces of the fusiform gyrus, mid fusiform sulcus, and collateral sulcus. Gray–white boundary, white solid lines. (*D*) Same as *C*, but resampled to 1-mm voxels using FreeSurfer. (*E*) Mean and individual subject (circles) estimates of CT using each measure. WM/GM, white/gray matter.

Second, histological analyses in postmortem brains validated our findings. Third, we found heterogeneous mechanisms of thinning across VTC. Different from face- and character-selective regions, there was no development of gray or white matter tissue properties of the CoS-places; instead, thinning in CoS-places was coupled with morphological changes. Thus, our study provides unique data that resolve theoretical debates regarding the development of CT.

Several innovations in our study have enabled the advancement of understanding mechanisms of thinning across development. First, the use of individual subject analyses with no spatial smoothing and tissue measurements across cortical depths has increased the precision of measurements from centimeters to millimeters and has enabled multimodal measurements (fMRI, qMRI, and dMRI) within each participant's brain. Second, leveraging our understanding of functional–structural relationships in VTC (37, 39), we identified relevant landmarks in ex vivo brain slices and validated in vivo measurements with histological measurements of myelin and CT. Third, we obtained independent measurements of T_1 from qMRI (19, 20) and MD from dMRI (22) in both gray and white matter. These complementary measures yielded consistent evidence supporting microstructural tissue growth in both tissue types. Fourth, our longitudinal data across 2 time points within the same individuals revealed a reduction in T_1 in the same fROIs that showed cross-sectional development. These data further strengthen and validate our cross-sectional findings. Thus, our findings not only provide striking empirical evidence supporting developmental theories of myelination in deeper gray matter and its adjacent white matter (2, 11, 13), but also underscore the utility of obtaining multimodal MR data in the same individual to glean insights into developmental mechanisms (6, 21).

Many prior studies have documented cortical thinning during childhood both cross-sectionally (1, 5) and longitudinally (2–4), which we replicate (Fig. 1 and *SI Appendix*, Figs. S2, S3, and S9). These studies have provided an important bird's-eye view of development as they elucidated developmental changes across the entire brain in large groups of participants. However, the mechanisms of developmental cortical thinning have been hypothetical until now. Some researchers have hypothesized that cortex thins during development due to synaptic pruning and cell loss (3). However, others argued that thinning observed with MRI is not due to tissue loss because there are developmental increases in gray and white matter volume (refs. 1, 2, and 56; see reviews in refs. 6 and 57) and changes to cortical T_1-weighted/T_2-weighted (T1w/T2w) metrics (53, 58). These results led researchers to suggest that developmental cortical thinning might be due to a shift in the gray–white boundary observed in MR images from increased myelin (14).

Our data provide evidence that increased myelination of axons during childhood is a key source of apparent cortical thinning in VTC after age 5. Three of our findings support this hypothesis for the development of face- and character-selective regions. First, we found age-related decreases in T_1 and MD in white matter adjacent to these regions. As myelin explains 90% of the variance in T_1 of white matter (59), this finding is likely explained by increased myelination. Second, in cortex, we found decreases in T_1 and MD far from the pial surface. Third, myelin staining in postmortem adult brain slices shows that myelin is prevalent in deep and intermediate cortical layers, especially in the FG. By validating in vivo measurements with histological measurements of myelin, we provide evidence for increased myelination during childhood rather than tissue loss. As myelin content affects the intensity of voxels in T_1-weighted anatomical MR images, our data suggest that increased myelin during development alters the gray–white matter contrast in MR images. That is, in children's brains that are less myelinated, the apparent gray–white boundary may be pushed into the adjacent hypomyelinated white matter. While our data suggest that myelin is a key contributor to T_1, our prior measurements and simulations also indicate that tissue growth in the gray matter affecting T_1 cannot be exclusively due to myelin increases (27). Growth in additional microstructures including glia (23, 60), dendritic arbors, synapses (61), and iron development in glia and myelin (21) also likely contribute to T_1 development in the gray matter.

Our data of developmental decreases in cortical T_1, both cross-sectionally and longitudinally, are consistent with prior cross-sectional studies of cortical development using myelin water fraction in infants (62), as well as studies using T_1w/T_2w imaging showing age-related development of this ratio from childhood up to 35 y of age (53, 58). While the T1w/T2w ratio is thought to be correlated with myelination (63, 64), it reflects a complex mix of tissue properties including iron, myelin, cell density, and water content, and thus, it may not provide an optimal measure of myelination (65). Partial voluming effects may also misclassify voxels to gray or white matter (53), further complicating interpretation of developmental effects. By measuring T_1 and MD across cortical depths, from the pial surface into the adjacent white matter, our measurements circumvent these issues.

Likewise, our finding of reduced T_1 and MD in the FDWM, adjacent to the developing cortex, is consistent with prior in vivo measurements suggesting myelination of white matter tracts across development (22, 24, 56, 66–69). Different from prior studies, which examined development of overall white matter properties of large-scale fascicles of the brain, we examine development of white matter properties adjacent to the developing cortex.

We acknowledge that a limitation of our study is the lack of histological pediatric data to validate in vivo estimates of CT in children. However, pediatric ex vivo data are scarce and challenging to obtain. Nonetheless, we are hopeful that future histological measurements in pediatric tissue will become available and can be used to 1) verify in vivo measurements of CT in children, and 2) determine whether development of myelin from childhood to adulthood shifts the apparent gray–white matter boundary deeper into cortex, or from hypomyelinated white matter to the actual gray–white matter interface. In the following subsections, we address 3 questions that arise from our findings.

First, why are there differences in the location of the largest developmental variations in T_1 vs. MD? The largest variation in MD was near the gray–white matter boundary, whereas that in T_1 was at the midcortical depth. We hypothesize that this difference arises from different microstructural mechanisms that affect T_1 and MD. The mean diffusivity of water molecules is affected by the physical hindrance generated by the axons' structure and spatial organization. As axons are more directionally structured in the white matter than in gray matter, the effects of developmental increases in myelination on MD may be larger in the white than gray matter. Furthermore, as the definition of the gray–white boundary from MRI is somewhat tentative, the developments in MD may appear to extend to gray matter close to the gray–white boundary. In contrast, T_1 in the gray matter depends on macromolecular tissue volume and the physiochemical properties of the tissue (19, 59). Our ex vivo analysis (Fig. 6) shows that cortical layers, especially layer IV, are highly myelinated in adulthood (see dark band in the cortex in Fig. 6*D*). Thus, if there are large developmental effects in myelination of the input axons, they may have a profound effect on T_1 in intermediate cortical depths. Thus, measurements of T_1 and MD provide complementary insights into microstructural development.

Second, is it possible that developmental pruning still occurs in VTC? While we did not find empirical evidence for pruning in VTC, pruning may still occur under 1 of 3 scenarios. One possibility is that pruning occurs earlier in development, e.g., during infancy (7, 8), but not after age 5. A second possibility is that pruning effects on T_1 and MD after age 5 are smaller in magnitude compared to effects of myelination; thus, the net effect on MRI measurements is dominated by myelin changes. A third possibility is that the present voxel resolution and field strength do not have sufficient sensitivity to measure pruning-related tissue loss. Work in nonhuman primates, however, has shown that spinogenesis and dendritic growth outpace pruning in macaque inferotemporal cortex (61, 70), which is homologous to human VTC. Future measurements with high-field MRI, equivolume models, submillimeter resolution, and ex vivo measurements in pediatric brains can test these possibilities (71).

Third, what may explain the differential mechanisms of cortical thinning across VTC? An interesting finding in our study is that different mechanisms underlie apparent thinning in face- and character-selective cortices compared to place-selective cortex, which is merely 2 cm away. In CoS-places, there was no development in either gray or white matter tissue properties. Instead, CT was correlated with the curvature of CoS-places and the SA of CoS. This suggests that the CoS may stretch and deepen across development, resulting in thinning as the same volume is divided across a larger surface area, which can be tested in future research. Changes in morphology during childhood may be due to mechanical forces including axonal tension (15), cytoarchitectural patterning (72), and differential white and gray matter properties (16). Our findings that morphological changes play a role in thinning also highlight that mechanical forces, which are a relatively overlooked factor of brain development after birth, should be considered not only during embryonic development, but also during childhood development.

One option to consider given the differences between place- and face-selective regions is that different mechanisms may affect development of sulci vs. gyri. However, our data suggest that this is not the case. While both CoS-places and mOTS-characters are in sulci, the latter exhibits tissue growth, but the former does not. Another possibility is that differences across VTC fROIs may reflect interplay between functional and structural development. Face- (27, 29–31, 34, 35) and character-selective ROIs (32, 33, 35, 73) show a protracted development compared to object- and place-selective ROIs in VTC. Research on oligodendrocytes and their progenitor cells indicate that development of myelin is activity dependent (74). Here, we propose an intriguing hypothesis: Cortical regions that exhibit protracted functional development will exhibit protracted myelin development, and consequently, prolonged apparent cortical thinning.

In summary, a major goal of neuroscience is to understand mechanisms of brain development. Our study demonstrates the feasibility of evaluating in vivo tissue properties in gray and white matter in children and adults using 3-T MRI. Critically, our study underscores the significance of multimodal measurements of microstructural and morphological changes of brain tissue across childhood development. As increased myelin during development changes the gray–white matter contrast in MR images, our data suggest that it results in apparent cortical thinning. Our findings have broad implications for large-scale studies of brain development including the Pediatric Imaging Neurocognition and Genetics Data Repository (75), the Adolescent Brain Cognitive Development study (76), and the HCP data (54) that use algorithms based on the intensity of MR images to estimate CT. Importantly, since these high-impact and large-scale studies will influence future policies that promote the health and well-being of children, our study proposes that multimodal (77) advanced qMRI and dMRI methods in combination with high-resolution 7-T whole-brain scans of ex vivo tissue (78) are exciting avenues to advance understanding of brain development. Finally, because apparent cortical thinning is pervasive during childhood and broadly throughout the life span, our data have key ramifications for understanding typical (79) and atypical brain development, as well as clinical conditions (80, 81) implicating myelin and morphology.

Materials and Methods

Participants. Twenty-seven children (14 females, ages 5 to 12) and 30 adults (11 females, ages 22 to 28) participated in our study. Children were recruited from the Palo Alto, California, school district, through flyers and online advertisements. Adult subjects are Stanford University affiliates. All subjects had normal or corrected-to-normal vision and provided written, informed consent. Protocols were approved by the Stanford Internal Review Board on Human Subjects.

Scanning Procedures. All subjects participated in multiple scanning sessions, on different days, to obtain qMRI, dMRI, and fMRI data. Children underwent a training session, prior to scanning, inside an MRI scanner simulator to remain still inside the scanner. All in vivo data were acquired using a 3-T GE Signa MRI scanner at Stanford University.

qMRI data. Subjects were scanned using methods described in our prior work (27). We used spin-echo inversion recovery with an echo-planar imaging (EPI), read-out (SEIR-EPI with TR = 3 s), and 2-mm^2 in-plane resolution (slice thickness, 4 mm). qMRI parameters were measured from spoiled-gradient echo images acquired with different flip angles (α = 4°, 10°, 20° and 30°; repetition time [TR] = 14 ms; echo time [TE] = 2.4 ms) and a voxel resolution of 0.8 × 0.8 × 1 mm^3 (resampled to 1-mm^3 isotropic). The TE was set to minimum full; inversion times were 50, 400, 1,200, and 2,400 ms. We generated whole-brain T_1-weighted anatomy, T_1 maps, and MTV maps (full procedure: https://github.com/mezera/mrQ) (19).

Generation of cortical surfaces, CT maps, and curvature maps. FreeSurfer's (FS v5.3) segmentation algorithm (http://surfer.nmr.mgh.harvard.edu/) was used to generate cortical surfaces from T_1 images, CT maps, and curvature maps. White matter surfaces were manually fixed for missing or mislabeled voxels using ITK-SNAP (http://www.itksnap.org/pmwiki/pmwiki.php). CT is measured as the distance between the gray–white boundary and pial surface (45). Curvature maps quantify curvature magnitude at each vertex and if the vertex is on a sulcus or gyrus.

dMRI data. In each subject, we obtained 2 whole-brain, diffusion-weighted, dual-spin echo-sequence (60 slices; TE = 96.8 ms; TR = 8,000 ms; 96 diffusion directions; b2000s/mm^2; voxel size, 2 × 2 × 2 mm^3) as in our prior work (47) (*SI Appendix*). Analyses were done using mrDiffusion (https://github.com/vistalab/vistasoft). Tensors were fit to each voxel using a least-squares algorithm, and MD maps were obtained from the tensors files.

fMRI data. Data were acquired using a T_2*-sensitive gradient echo spiral pulse sequence with a resolution of 2.4 × 2.4 × 2.4 mm^3, TR = 1,000 ms, TE = 30 ms, flip angle = 76°, and field of view = 192 mm, based on our prior work (27, 34, 35, 43).

Functional localizer. To localize fROIs, subjects participated in a localizer experiment as in our prior work (27, 34, 35, 43) (*SI Appendix*). Subjects viewed gray-scale stimuli, which were blocked by category. Images included 2 subtypes

from 5 categories: characters (numbers and pseudowords), bodies (limbs and headless bodies), human faces (child and adult faces), places (houses and indoor scenes), and objects (guitars and cars) (*SI Appendix*, Fig. S1*A*). Localizer data were analyzed using mrVista (https://github.com/vistalab/vistasoft). Data were not spatially smoothed and were analyzed in each subject's native brain space.

Definition of fROIs in VTC. Category-selective voxels were defined as voxels that responded more to images of one category than those of other categories ($t > 3$, voxel level). We defined face-, character-, and place-selective fROIs in each participant as in our prior studies (27, 34, 35, 43) (*SI Appendix*).

In Vivo Cross-Sectional Analyses Examining Anatomical Features of Functional Regions.

Analysis of CT in fROIs. Each subject's FreeSurfer's CT maps were transformed to volume nifti files using FreeSurfer's *mri_surf2vol* algorithm. We first averaged in each subject CT within each fROI, and then averaged CT across subjects within an age group.

Analysis of T_1, MTV, and MD in FDWM. Each subject's fROI was extended into its neighboring white matter by 5 mm, to obtain T_1, MTV, and MD measures in its FDWM (*SI Appendix*). Mean T_1, MTV, and MD were calculated for the FDWM and averaged across subjects within an age group. Statistical analyses were performed using repeated-measures ANOVAs.

Analysis of T_1/MD by intracortical depth. Using FreeSurfer's *mri_surf2vol* algorithm, each subject's white matter surface was converted to volume niftis. The volume was projected into gray matter at increasing 20% steps, starting from 2 locations below the gray–white boundary (to include white matter just below the boundary) to 2 locations above the pial surface (to include the entire pial surface; *SI Appendix*). For each subject's fROI, we averaged T_1 values of the voxels that intersected with each cortical layer and obtained T_1 per cortical depth. Similar analysis was conducted for MD, with the exception that the cortex was divided into 8 rather than 10 steps, as MD maps were 2-mm voxel resolution. We fitted logistic functions to subject's T_1 curves and linear functions to MD curves, and statistical analysis was performed on the parameters of the functions.

In Vivo Longitudinal Data Analysis. Eighteen out of 26 children (10 females; ages, 5 to 12) returned after 1.42 ± 0.15 y following the first qMRI session for a second qMRI session, which used the same MR scanner and analysis pipelines as session 1. To test whether our data replicate prior longitudinal data in anatomical parcellations (2), we generated CT maps for year 2 data using FreeSurfer and estimated CT in anatomical parcellations of the FG, OTS, and CoS. Given our cross-sectional findings that T_1 decreases in face and character fROIs, we also tested whether T_1 decreases within the same child's fROIs across ∼1.5. Each subject's T_1 map from year 2 was aligned to T_1 map from year 1 (*SI Appendix*). We then extracted mean T_1 per fROI (face-, place- and character-selective) and year. Statistical analysis was performed using ANOVAs.

Histology (Postmortem Tissue Blocks). Blocks of 5 postmortem brains were provided by the Brain Banking Centre Leipzig of the German Brain-Net (GZ 01GI9999-01GI0299), operated by the Paul Flechsig Institute of Brain Research (University of Leipzig) (*SI Appendix*, Table S2). All tissue blocks contained a part of the calcarine fissure, lateral FG/MFS where face-selective regions reside, and CoS where the place-selective region resides.

Tissue sectioning. Tissue blocks were cryoprotected in 30% sucrose/PBS with 0.1% sodium azide. Sections of 30-μm thickness were made on a cryomicrotome (Leica SM2000R with freezing unit Zeiss KS34) and collected in PBS with 0.1% sodium azide.

Myelin staining. Sections were rehydrated in distilled water and stained following the classical Gallyas protocol (48) with modifications (82). To assure the complete visualization of myelin fibers, including thin fibers, the developing step was extended to 40 min (*SI Appendix*). All images were obtained under equal conditions to ensure comparable data for the optometric processing. Obtained RGB maps were logarithmically transformed using the Lambert–Beer transformation and averaged across 3 color channels with corresponding weights to measure OD, which is proportional to the density of staining chromophore and reflects local myelin density in the tissue (i.e., $OD = 0.8*R + 1.2*G + 1.5*B$, where R, G, B are the red, green, and blue channels in a .tiff image file).

Nissl staining. To visualize the neuronal layers in the cortex, Nissl substance in neurons was stained with 0.1% cresyl violet in acetate buffer, followed by differentiation in 70% ethanol. The section of slices used for Nissl staining was adjacent to the section used for myelin silver staining. Each Nissl and myelin slice had a thickness of 30 μm.

MR scanning. MR scanning of tissue samples was performed on a 7-T Siemens scanner (Magnetom; Siemens). Multiparameter mapping (MPM) method was used to acquire quantitative maps of longitudinal relaxation rate R_1 and effective transverse relaxation rate R_2* (83). hMRI Toolbox (https://hmri-group.github.io/hMRI-toolbox/) was used to reconstruct R_2*, PD, and R_1 maps (84).

Analysis of adult ex vivo myelin data vs. adult in vivo T_1 data in face- and place-selective cortex. For each myelin slice, we divided the cortex into equidistant depths from the pial surface to white matter. We achieved this by drawing a midline across depths in FG/MFS and CoS, and then projecting equidistant depths along the midline normal in 2 steps: 1) from midline to pial surface and 2) midline to white matter. We obtained mean OD (myelin density) at each depth (OD at each point was normalized with respect to OD in white matter) per region.

Measuring CT in Nissl and myelin stains. To test whether myelin and Nissl staining at micrometer resolution provide the same estimates of CT, we measured CT in the regions of interest independently from Nissl and myelin slices. As far as possible, we closely matched the slices across stains. CT was estimated using Netscope (https://www.netscope.de/home.html) and was measured at multiple points along the FG/MFS and CoS (*SI Appendix*, Fig. S12).

Data Availability. Code relevant for analysis and source data (Figs. 1–8) will be made available upon request. The majority of the code is available at https://github.com/vistalab/vistasoft.

ACKNOWLEDGMENTS. This research was funded by NIH Grants 1R01EY022318 and 1R01EY023915 (to K.G.-S.), Grant 5T32EY020485 (to V.S.N.), and National Research Service Award F31EY027201 (to J.G.). We thank Prof. Dr. Thomas Arendt from the Paul Flechsig Institute of Brain Research, University of Leipzig, for providing postmortem brain samples. This project was supported by the European Research Council under the European Union's Seventh Framework Programme (FP7/2007-2013)/European Research Council Grant Agreement 616905, and Bundesministerium für Bildung und Forschung (01EW1711A and B) in the framework of ERA-NET NEURON.

1. E. R. Sowell *et al*., Mapping cortical change across the human life span. *Nat. Neurosci.* **6**, 309–315 (2003).
2. E. R. Sowell *et al*., Longitudinal mapping of cortical thickness and brain growth in normal children. *J. Neurosci.* **24**, 8223–8231 (2004).
3. N. Gogtay *et al*., Dynamic mapping of human cortical development during childhood through early adulthood. *Proc. Natl. Acad. Sci. U.S.A.* **101**, 8174–8179 (2004).
4. P. Shaw *et al*., Intellectual ability and cortical development in children and adolescents. *Nature* **440**, 676–679 (2006).
5. I. K. Amlien *et al*., Organizing principles of human cortical development—thickness and area from 4 to 30 years: Insights from comparative primate neuroanatomy. *Cereb. Cortex* **26**, 257–267 (2016).
6. K. B. Walhovd, A. M. Fjell, J. Giedd, A. M. Dale, T. T. Brown, Through thick and thin: A need to reconcile contradictory results on trajectories in human cortical development. *Cereb. Cortex* **27**, 1472–1481 (2017).
7. P. R. Huttenlocher, Synaptic density in human frontal cortex—developmental changes and effects of aging. *Brain Res.* **163**, 195–205 (1979).
8. P. Rakic, J. P. Bourgeois, M. F. Eckenhoff, N. Zecevic, P. S. Goldman-Rakic, Concurrent overproduction of synapses in diverse regions of the primate cerebral cortex. *Science* **232**, 232–235 (1986).
9. Z. Petanjek, M. Judas, I. Kostović, H. B. Uylings, Lifespan alterations of basal dendritic trees of pyramidal neurons in the human prefrontal cortex: A layer-specific pattern. *Cereb. Cortex* **18**, 915–929 (2008).
10. P. Flechsig, *Anatomie des Menschen Gehirns und Rückenmarksauf Myelogenetischer Grudlage* (Georg Thime, Leipzig, 1920), p. 4.
11. P. L. Yakovlev, A. R. Lecours, "The myelogenetic cycles of regional maturation of the Brain" in *Regional Development of the Brain in Early Life*, A. Minkowski, Ed. (Blackwell, Oxford, 1967).
12. F. M. Benes, M. Turtle, Y. Khan, P. Farol, Myelination of a key relay zone in the hippocampal formation occurs in the human brain during childhood, adolescence, and adulthood. *Arch. Gen. Psychiatry* **51**, 477–484 (1994).
13. D. J. Miller *et al*., Prolonged myelination in human neocortical evolution. *Proc. Natl. Acad. Sci. U.S.A.* **109**, 16480–16485 (2012).
14. D. H. Salat *et al*., Age-associated alterations in cortical gray and white matter signal intensity and gray to white matter contrast. *Neuroimage* **48**, 21–28 (2009).
15. D. C. Van Essen, A tension-based theory of morphogenesis and compact wiring in the central nervous system. *Nature* **385**, 313–318 (1997).
16. T. Tallinen, J. Y. Chung, J. S. Biggins, L. Mahadevan, Gyrification from constrained cortical expansion. *Proc. Natl. Acad. Sci. U.S.A.* **111**, 12667–12672 (2014).
17. K. E. Garcia, C. D. Kroenke, P. V. Bayly, Mechanics of cortical folding: Stress, growth and stability. *Philos. Trans. R. Soc. Lond. B Biol. Sci.* **373**, 20170321 (2018).
18. L. J. Hogstrom, L. T. Westlye, K. B. Walhovd, A. M. Fjell, The structure of the cerebral cortex across adult life: Age-related patterns of surface area, thickness, and gyrification. *Cereb. Cortex* **23**, 2521–2530 (2013).
19. A. Mezer *et al*., Quantifying the local tissue volume and composition in individual brains with magnetic resonance imaging. *Nat. Med.* **19**, 1667–1672 (2013).

20. A. Lutti, F. Dick, M. I. Sereno, N. Weiskopf, Using high-resolution quantitative mapping of R1 as an index of cortical myelination. *Neuroimage* **93**, 176–188 (2014).
21. L. J. Edwards, E. Kirilina, S. Mohammadi, N. Weiskopf, Microstructural imaging of human neocortex in vivo. *Neuroimage* **182**, 184–206 (2018).
22. C. Beaulieu, The basis of anisotropic water diffusion in the nervous system—a technical review. *NMR Biomed.* **15**, 435–455 (2002).
23. R. J. Zatorre, R. D. Fields, H. Johansen-Berg, Plasticity in gray and white: Neuroimaging changes in brain structure during learning. *Nat. Neurosci.* **15**, 528–536 (2012).
24. J. D. Yeatman, B. A. Wandell, A. A. Mezer, Lifespan maturation and degeneration of human brain white matter. *Nat. Commun.* **5**, 4932 (2014).
25. J. Dinse *et al*., A cytoarchitecture-driven myelin model reveals area-specific signatures in human primary and secondary areas using ultra-high resolution in-vivo brain MRI. *Neuroimage* **114**, 71–87 (2015).
26. C. Vogt, O. Vogt, Ergebnisse unserer hirnforschung.1.-4. Mitteilung. *J. Psychol. Neurol.* **25**, 279–461 (1919).
27. J. Gomez *et al*., Microstructural proliferation in human cortex is coupled with the development of face processing. *Science* **355**, 68–71 (2017).
28. K. J. Whitaker *et al*.; NSPN Consortium, Adolescence is associated with genomically patterned consolidation of the hubs of the human brain connectome. *Proc. Natl. Acad. Sci. U.S.A.* **113**, 9105–9110 (2016).
29. K. S. Scherf, M. Behrmann, K. Humphreys, B. Luna, Visual category-selectivity for faces, places and objects emerges along different developmental trajectories. *Dev. Sci.* **10**, F15–F30 (2007).
30. M. V. Peelen, B. Glaser, P. Vuilleumier, S. Eliez, Differential development of selectivity for faces and bodies in the fusiform gyrus. *Dev. Sci.* **12**, F16–F25 (2009).
31. G. Golarai *et al*., Differential development of high-level visual cortex correlates with category-specific recognition memory. *Nat. Neurosci.* **10**, 512–522 (2007).
32. M. Ben-Shachar, R. F. Dougherty, G. K. Deutsch, B. A. Wandell, The development of cortical sensitivity to visual word forms. *J. Cogn. Neurosci.* **23**, 2387–2399 (2011).
33. Z. M. Saygin *et al*., Connectivity precedes function in the development of the visual word form area. *Nat. Neurosci.* **19**, 1250–1255 (2016).
34. V. S. Natu *et al*., Development of neural sensitivity to face identity correlates with perceptual discriminability. *J. Neurosci.* **36**, 10893–10907 (2016).
35. M. Nordt *et al*., Learning to read increases the informativeness of distributed ventral temporal responses. *Cereb. Cortex* **29**, 3124–3139 (2019).
36. K. Grill-Spector, G. Golarai, J. Gabrieli, Developmental neuroimaging of the human ventral visual cortex. *Trends Cogn. Sci. (Regul. Ed.)* **12**, 152–162 (2008).
37. K. S. Weiner *et al*., The mid-fusiform sulcus: A landmark identifying both cytoarchitectonic and functional divisions of human ventral temporal cortex. *Neuroimage* **84**, 453–465 (2014).
38. K. S. Weiner *et al*., Defining the most probable location of the parahippocampal place area using cortex-based alignment and cross-validation. *Neuroimage* **170**, 373–384 (2018).
39. K. S. Weiner *et al*., The cytoarchitecture of domain-specific regions in human high-level visual cortex. *Cereb. Cortex* **27**, 146–161 (2017).
40. N. Kanwisher, J. McDermott, M. M. Chun, The fusiform face area: A module in human extrastriate cortex specialized for face perception. *J. Neurosci.* **17**, 4302–4311 (1997).
41. K. S. Weiner, K. Grill-Spector, Sparsely-distributed organization of face and limb activations in human ventral temporal cortex. *Neuroimage* **52**, 1559–1573 (2010).
42. L. Cohen *et al*., The visual word form area: Spatial and temporal characterization of an initial stage of reading in normal subjects and posterior split-brain patients. *Brain* **123**, 291–307 (2000).
43. A. Stigliani, K. S. Weiner, K. Grill-Spector, Temporal processing capacity in high-level visual cortex is domain specific. *J. Neurosci.* **35**, 12412–12424 (2015).
44. R. Epstein, N. Kanwisher, A cortical representation of the local visual environment. *Nature* **392**, 598–601 (1998).
45. B. Fischl, A. M. Dale, Measuring the thickness of the human cerebral cortex from magnetic resonance images. *Proc. Natl. Acad. Sci. U.S.A.* **97**, 11050–11055 (2000).
46. C. V. Von Economo, *The Cytoarchitectonics of the Human Cerebral Cortex* (Oxford Medical Publications, London, 1929).
47. J. Gomez *et al*., Functionally defined white matter reveals segregated pathways in human ventral temporal cortex associated with category-specific processing. *Neuron* **85**, 216–227 (2015).
48. F. Gallyas, Silver staining of myelin by means of physical development. *Neurol. Res.* **1**, 203–209 (1979).
49. S. Bok, Der Ein fl uß der in den Furchen und Windungen auftretenden Krümmungen der Großhirnrinde auf die Rindenarchitektur. *Z. Gesamte Neurol. Psychiatr.* **121**, 682–750 (1929).
50. M. D. Waehnert *et al*., Anatomically motivated modeling of cortical laminae. *Neuroimage* **93**, 210–220 (2014).
51. B. Fischl, M. I. Sereno, R. B. Tootell, A. M. Dale, High-resolution intersubject averaging and a coordinate system for the cortical surface. *Hum. Brain Mapp.* **8**, 272–284 (1999).
52. H. Lemaitre *et al*., Normal age-related brain morphometric changes: Nonuniformity across cortical thickness, surface area and gray matter volume? *Neurobiol. Aging* **33**, 617.e1–617.e9 (2012).
53. R. Shafee, R. L. Buckner, B. Fischl, Gray matter myelination of 1555 human brains using partial volume corrected MRI images. *Neuroimage* **105**, 473–485 (2015).
54. D. C. Van Essen *et al*.; WU-Minn HCP Consortium, The WU-Minn Human Connectome Project: An overview. *Neuroimage* **80**, 62–79 (2013).
55. N. Zaretskaya, B. Fischl, M. Reuter, V. Renvall, J. R. Polimeni, Advantages of cortical surface reconstruction using submillimeter 7 T MEMPRAGE. *Neuroimage* **165**, 11–26 (2018).
56. C. K. Tamnes *et al*., Brain maturation in adolescence and young adulthood: Regional age-related changes in cortical thickness and white matter volume and microstructure. *Cereb. Cortex* **20**, 534–548 (2010).
57. T. T. Brown, T. L. Jernigan, Brain development during the preschool years. *Neuropsychol. Rev.* **22**, 313–333 (2012).
58. H. Grydeland, K. B. Walhovd, C. K. Tamnes, L. T. Westlye, A. M. Fjell, Intracortical myelin links with performance variability across the human lifespan: Results from T1- and T2-weighted MRI myelin mapping and diffusion tensor imaging. *J. Neurosci.* **33**, 18618–18630 (2013).
59. C. Stüber *et al*., Myelin and iron concentration in the human brain: A quantitative study of MRI contrast. *Neuroimage* **93**, 95–106 (2014).
60. B. A. Barres, M. C. Raff, Proliferation of oligodendrocyte precursor cells depends on electrical activity in axons. *Nature* **361**, 258–260 (1993).
61. G. N. Elston, I. Fujita, Pyramidal cell development: Postnatal spinogenesis, dendritic growth, axon growth, and electrophysiology. *Front. Neuroanat.* **8**, 78 (2014).
62. S. C. Deoni, D. C. Dean, 3rd, J. Remer, H. Dirks, J. O'Muircheartaigh, Cortical maturation and myelination in healthy toddlers and young children. *Neuroimage* **115**, 147–161 (2015).
63. M. F. Glasser, D. C. Van Essen, Mapping human cortical areas in vivo based on myelin content as revealed by T1- and T2-weighted MRI. *J. Neurosci.* **31**, 11597–11616 (2011).
64. M. F. Glasser, M. S. Goyal, T. M. Preuss, M. E. Raichle, D. C. Van Essen, Trends and properties of human cerebral cortex: Correlations with cortical myelin content. *Neuroimage* **93**, 165–175 (2014).
65. D. Carey *et al*., Quantitative MRI provides markers of intra-, inter-regional, and age-related differences in young adult cortical microstructure. *Neuroimage* **182**, 429–440 (2018).
66. C. Lebel, L. Walker, A. Leemans, L. Phillips, C. Beaulieu, Microstructural maturation of the human brain from childhood to adulthood. *Neuroimage* **40**, 1044–1055 (2008).
67. L. T. Westlye *et al*., Life-span changes of the human brain white matter: Diffusion tensor imaging (DTI) and volumetry. *Cereb. Cortex* **20**, 2055–2068 (2010).
68. C. Lebel, C. Beaulieu, Longitudinal development of human brain wiring continues from childhood into adulthood. *J. Neurosci.* **31**, 10937–10947 (2011).
69. S. C. Deoni *et al*., Mapping infant brain myelination with magnetic resonance imaging. *J. Neurosci.* **31**, 784–791 (2011).
70. G. N. Elston, T. Oga, I. Fujita, Spinogenesis and pruning scales across functional hierarchies. *J. Neurosci.* **29**, 3271–3275 (2009).
71. R. Turner, D. De Haan, Bridging the gap between system and cell: The role of ultra-high field MRI in human neuroscience. *Prog. Brain Res.* **233**, 179–220 (2017).
72. B. Fischl *et al*., Cortical folding patterns and predicting cytoarchitecture. *Cereb. Cortex* **18**, 1973–1980 (2008).
73. G. Dehaene-Lambertz, K. Monzalvo, S. Dehaene, The emergence of the visual word form: Longitudinal evolution of category-specific ventral visual areas during reading acquisition. *PLoS Biol.* **16**, e2004103 (2018).
74. R. D. Fields, A new mechanism of nervous system plasticity: Activity-dependent myelination. *Nat. Rev. Neurosci.* **16**, 756–767 (2015).
75. T. L. Jernigan *et al*.; Pediatric Imaging, Neurocognition and Genetics Study, The Pediatric Imaging, Neurocognition, and Genetics (PING) data repository. *Neuroimage* **124**, 1149–1154 (2016).
76. B. J. Casey *et al*.; ABCD Imaging Acquisition Workgroup, The Adolescent Brain Cognitive Development (ABCD) study: Imaging acquisition across 21 sites. *Dev. Cogn. Neurosci.* **32**, 43–54 (2018).
77. C. L. Tardif *et al*., Advanced MRI techniques to improve our understanding of experience-induced neuroplasticity. *Neuroimage* **131**, 55–72 (2016).
78. Edlow *et al*., Tesla MRI of the ex vivo human brain at 100 micron resolution. bioRxiv: 10.1101/649822 (31 May 2019).
79. B. Deen *et al*., Organization of high-level visual cortex in human infants. *Nat. Commun.* **8**, 13995 (2017).
80. Y. Ma *et al*., Cortical thickness abnormalities associated with dyslexia, independent of remediation status. *Neuroimage Clin.* **7**, 177–186 (2014).
81. M. Sailer *et al*., Focal thinning of the cerebral cortex in multiple sclerosis. *Brain* **126**, 1734–1744 (2003).
82. A. L. Pistorio, S. H. Hendry, X. Wang, A modified technique for high-resolution staining of myelin. *J. Neurosci. Methods* **153**, 135–146 (2006).
83. N. Weiskopf *et al*. Quantitative multi-parameter mapping of R1, PD*, MT, and R2* at 3T: A multi-center validation. *Front. Neurosci.* **7**, 95 (2013).
84. K. Tabelow *et al*., hMRI—a toolbox for quantitative MRI in neuroscience and clinical research. *Neuroimage* **194**, 191–210 (2019).